ACS OMEGA

Open Access

http://pubs.acs.org/journal/acsodf

Article

Streaming Current for Surfaces Covered by Square and Hexagonal Monolayers of Spherical Particles

Jerzy Blawzdziewicz,* Zbigniew Adamczyk, and Maria L. Ekiel-Jeżewska*

Cite This: *ACS Omega* 2023, 8, 44717−44723

Read Online

ACCESS | Metrics & More | Article Recommendations

ABSTRACT: The interface and particle contributions to the streaming current of flat substrates covered with ordered square or hexagonal monolayers of spherical particles were theoretically evaluated for particle coverage up to close packing. The exact numerical results were approximated using fitting functions that contain exponential and linear terms to account for hydrodynamic screening and charge convection from the particle surfaces exposed to external flow. According to our calculations, the streaming currents for the ordered and random particle arrangements differ within a typical experimental error. Thus, streaming-current measurements, supplemented with our fitting functions, can be conveniently used to evaluate the particle coverage without detailed knowledge of the particle distribution. Our results for equal interface and particle ζ-potentials indicate that roughness can reduce the streaming current by more than 30%, even in the limit of the small size of spherical roughness asperities.

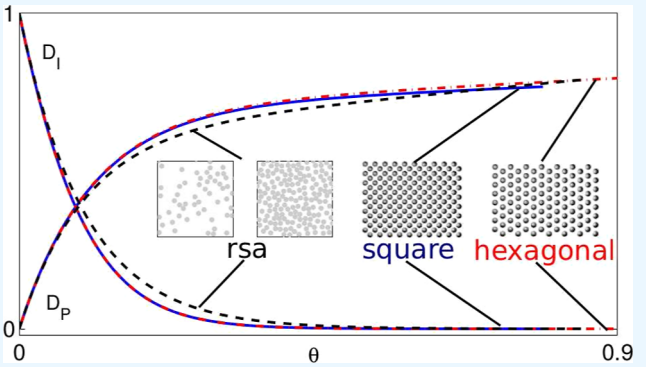

INTRODUCTION

Deposition of nano- or microscale particles on solid surfaces is of great importance in a variety of fields of science and technology.[1−10] Particle-covered surfaces are used, for example, as functional materials in electro-optical devices,[11−13] biosensors,[14−17] biomaterials,[18,19] and plasmon-resonance spectroscopy devices.[1] In other applications (e.g., medical devices and membrane filtration systems), particle deposition needs to be prevented to avoid surface fouling.[20]

A promising class of methods that can be used in situ to monitor deposition of nanoparticle monolayers under various physicochemical conditions consists of electrokinetic methods based on the measurements of the streaming current (or its derivative parameter, the streaming potential).[3,8] For example, these techniques were applied to quantitatively evaluate the deposition kinetics[9,21,22] and to determine the mechanisms of globular protein adsorption on solid/electrolyte interfaces.[23−25]

While a continuous measurement of the streaming current (or streaming potential) provides a convenient means for monitoring the deposition process, an accurate quantitative interpretation of the measurement results is not straightforward. This difficulty stems from the fact that the streaming current depends not only on the particle coverage (area fraction) θ of the particle monolayer but also on its other geometrical characteristics, such as particle shape and distribution. Thus, to fully utilize the power of the electrokinetic methods for monitoring of particle deposition, a thorough analysis of this dependence is required.

Recently, an accurate theoretical method has been developed for evaluating the streaming current produced by an arbitrary distribution of spherical particles adsorbed on a planar surface.[26,27] This method has been used to determine the streaming current for equilibrium[26,27] and random-sequential adsorption (RSA)[27] distributions of the deposited particles. Accurate theoretical expressions for the streaming current as a function of the area fraction of adsorbed particles were provided[26,27] and successfully used to interpret electrokinetic measurements under conditions where particle adsorption produces a disordered monolayer.[3,9]

The disordered equilibrium and RSA distributions commonly occur in adsorption processes[28] but other distributions are also of a significant importance. In particular, ordered square and hexagonal periodic distributions of particles deposited on solid substrates (see Figure 1 reprinted from refs 29 and 30) have been produced using a variety of experimental procedures, including the electric-field-enhanced

Received: July 31, 2023
Revised: October 14, 2023
Accepted: October 19, 2023
Published: November 14, 2023

https://doi.org/10.1021/acsomega.3c05603
ACS Omega 2023, 8, 44717−44723

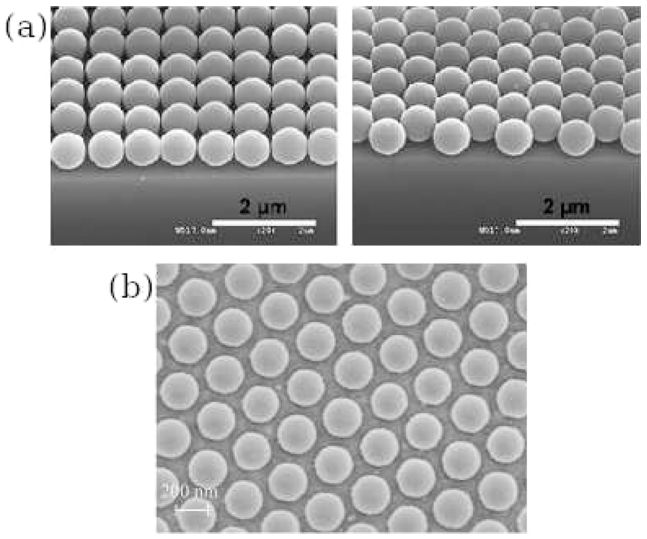

Figure 1. Examples of experimentally assembled 2D ordered monolayers of spherical particles. (a) SEM micrograph of a square (left) and hexagonal (right) close-packed array of silica microspheres on a Si wafer. The images are reprinted with permission from Khanh and Yoon,[29] Copyright 2009 American Chemical Society. (b) SEM micrograph of a hexagonal monolayer of polystyrene nanospheres on the graphene substrate at an area fraction below close packing. The image reprinted with permission from Lotito and Zambelli,[30] Copyright 2015 Elsevier.

self-assembly (electrophoresis),[31,32] capillary-force-driven clustering,[33,34] and the Langmuir−Blodgett assembly at liquid air interfaces followed by particle monolayer transfer to solid substrates.[35] Such ordered structures can be used, for example, to develop band gap materials and optical filters, and therefore, they are of potentially large technological significance.

THEORETICAL METHODS

The main goal of the present work is to provide accurate numerical simulation data and convenient theoretical expressions for the streaming current for a planar interface covered with adsorbed spherical particles arranged on hexagonal and square ordered lattices. It is assumed that the Debye screening length λ is much smaller than the particle radius a_0, i.e., $\lambda/a_0 \ll 1$. The ζ-potentials of the particles and the interface are ζ_P and ζ_I, respectively. In practical applications, the ζ-potential of a planar interface can be evaluated from the uncompensated (electrokinetic) charge in the slip plane using the Gouy−Chapman formula,[36,37] and the ζ-potential of particles can be determined by employing microelectrophoretic techniques.[9]

The particle-covered interface (see schematic depicted in Figure 2) is subject to an external linear flow $\mathbf{v}_0 = \dot{\gamma} z \hat{\mathbf{e}}_x$ under Stokes-flow conditions. Here, $z = 0$ is the position of the interface, the fluid occupies the region $z > 0$, and $\hat{\mathbf{e}}_x$ is the unit vector along the flow direction x. The external linear flow is perturbed by the adsorbed particles; the resulting total flow $\mathbf{v}(\mathbf{r})$ satisfies the stick boundary conditions on the interface S_I and the particle surfaces S_k, $k = 1, ..., N$, where $\mathbf{r}$ is the position vector and N is the number of adsorbed particles.

As described in refs 26 and 27, the flow field $\mathbf{v}(\mathbf{r})$ convects the electrokinetic charge of the Debye double layer, producing the streaming current

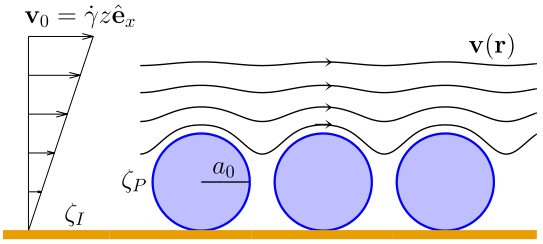

Figure 2. System geometry. A periodic array of spherical particles of radius a_0 and ζ-potential ζ_P is adsorbed on a planar surface of ζ-potential ζ_I. The particles are subject to external shear flow $\mathbf{v}_0 = \dot{\gamma} z \hat{\mathbf{e}}_x$, pointing in the x-direction and varying in the z-direction. The resulting fluid velocity field $\mathbf{v}(\mathbf{r})$ is represented by curved solid lines. For positions $\mathbf{r}$ close to the particle surface, $\mathbf{v}(\mathbf{r})$ is approximately tangential to the surface. In the regions between the particles, fluid flow is weak because of hydrodynamic screening.

$$I_s = \int_{\Delta S_c} \rho(\mathbf{r}) \mathbf{v}(\mathbf{r}) \cdot \hat{\mathbf{e}}_x \, dS \tag{1}$$

passing through the control surface $\Delta S_c = H \times l$, where H and l denote the surface dimensions in the z and y directions, respectively, and $\rho(\mathbf{r})$ is the charge density. We note that for a square and hexagonal symmetry of the particle monolayer, the streaming current eq 1 does not depend on the flow orientation with respect to the particle lattice.

Using the Poisson equation, averaging over the control volume, integrating by parts, and splitting the resulting surface integral into the interface and particle components, eq 1 can be reduced to the expression

$$\frac{I_s}{I_0} = D_I + \frac{\zeta_P}{\zeta_I} D_P \tag{2}$$

where

$$I_0 = -\epsilon \zeta_I l \dot{\gamma} \tag{3}$$

is the streaming current, defined in eq 1 for a particle-free interface, and

$$D_I = \frac{\theta}{\pi a_0^2 \dot{\gamma}} \frac{1}{N} \int_{S_I} \hat{\mathbf{e}}_z \cdot \nabla \mathbf{v}(\mathbf{r}) \cdot \hat{\mathbf{e}}_x \, dS \tag{4a}$$

$$D_P = \frac{\theta}{\pi a_0^2 \dot{\gamma}} \frac{1}{N} \sum_{k=1}^{N} \int_{S_k} \hat{\mathbf{n}}_k(\mathbf{r}) \cdot \nabla \mathbf{v}(\mathbf{r}) \cdot \hat{\mathbf{e}}_x \, dS \tag{4b}$$

are the interface and particle streaming-current contributions. Here, $\hat{\mathbf{n}}_k$ is the unit vector normal to the particle surface S_k (pointing into the fluid), and $\theta = \pi a_0^2 n$ is the surface coverage (area fraction) of the particle monolayer, where $n = N/A$ is the number of particles per unit area A.

As shown before,[26,27] the interface contribution can be expressed in terms of the total hydrodynamic force $F = \sum_{k=1}^{N} F_k$ acting on the particles in the direction of the ambient flow

$$D_I = 1 - \frac{\theta}{\pi \eta a_0^2 \dot{\gamma}} \frac{F}{N} \tag{5}$$

The particle contribution

$$D_P = \frac{\theta}{\pi \eta a_0^2 \dot{\gamma}} \frac{F - Q_P}{N} \tag{6}$$

https://doi.org/10.1021/acsomega.3c05603
ACS Omega 2023, 8, 44717−44723

Table 1. Interface Contributions A_I and D_I and Particle Contributions A_P and D_P to the Streaming Current I_s for Square and Hexagonal Particle Monolayers[a]

	square				hexagonal			
θ	A_I^{sq}	A_P^{sq}	D_I^{sq}	D_P^{sq}	A_I^{hex}	A_P^{hex}	D_I^{hex}	D_P^{hex}
0	10.20371	6.50975	1.000	0.000	10.20371	6.50975	1.000	0.000
0.05	8.662	5.548	0.567	0.277	8.679	5.557	0.566	0.278
0.10	6.918	4.485	0.308	0.448	6.939	4.496	0.306	0.450
0.15	5.564	3.671	0.165	0.551	5.580	3.680	0.163	0.552
0.20	4.563	3.070	0.087	0.614	4.570	3.077	0.086	0.615
0.25	3.821	2.620	0.045	0.655	3.821	2.627	0.045	0.657
0.30	3.261	2.274	0.022	0.682	3.256	2.283	0.023	0.685
0.35	2.831	2.004	0.009	0.701	2.824	2.014	0.012	0.705
0.40	2.493	1.788	0.003	0.715	2.486	1.800	0.006	0.720
0.45	2.222	1.612	0.000	0.726	2.216	1.627	0.003	0.732
0.50	2.002	1.467	−0.001	0.734	1.998	1.484	0.001	0.742
0.55	1.820	1.346	−0.001	0.740	1.818	1.365	0.000	0.751
0.60	1.668	1.243	−0.001	0.746	1.667	1.264	0.000	0.759
0.65	1.539	1.155	0.000	0.751	1.539	1.178	0.000	0.766
0.70	1.428	1.079	0.000	0.755	1.429	1.103	0.000	0.772
0.75	1.333	1.013	0.000	0.760	1.334	1.037	0.000	0.778
0.77	1.298	0.989	0.001	0.761				
0.80					1.250	0.980	0.000	0.784
0.85					1.177	0.928	0.000	0.789
0.90					1.111	0.882	0.000	0.794

[a]The results for $\theta = 0$ were obtained using the cluster-expansion method,[26] and the remaining data were evaluated from simulations of the electrokinetic flow in a square or hexagonal unit cell.

involves the average hydrodynamic force F and an additional term

$$Q_P = -\sum_k \int_{S_k} p(\mathbf{r})\hat{\mathbf{n}}_k(\mathbf{r})\cdot\hat{\mathbf{e}}_x \mathrm{d}S \tag{7}$$

related to the fluid pressure $p(\mathbf{r})$ at the surfaces S_k of all the particles $k = 1, ..., N$.[27]

In this paper, the hydrodynamic force acting on the particles F and the pressure contribution were determined using the Hydromultipole numerical algorithm, based on the multipole method of solving the Stokes equations.[38,39] The hydrodynamic wall effects were incorporated using the Cartesian representation method,[40−42] also employed in refs 26 and 27. The calculations were performed by using 2D periodic boundary conditions in the directions parallel to the interface. There is $N = 1$ particle in a unit cell for the square lattice and $N = 2$ particles for the hexagonal lattice.

RESULTS AND DISCUSSION

Our numerical results for the interface and particle contributions to the streaming current, D_I and D_P, are presented in Table 1 and Figure 3 for the square and hexagonal particle configurations. The results have been obtained[27] using a multipolar-expansion truncation order[38,39] $L = 9$ for the square lattice and $L = 12$ for the hexagonal lattice. The precision of the results is ±0.001. For each particle lattice, the data are presented for $\theta \lesssim \theta_{cp}$, where the close packing area fraction for the hexagonal lattice is $\theta_{cp} = \pi/(2\sqrt{3}) \approx 0.907$ and for the square lattice is $\theta_{cp} = \pi/4 \approx 0.785$.

In Table 1, we also provide the data for the associated functions

$$A_I(\theta) = \frac{1 - D_I(\theta)}{\theta}, \qquad A_P(\theta) = \frac{D_P(\theta)}{\theta} \tag{8}$$

In the low-area-fraction limit, $\theta \to 0$, the functions eq 8 tend to the leading-order virial expansion coefficients, D_I^0 and D_P^0, in the area-fraction expansion of D_I and D_P

$$D_I = 1 - D_I^0\theta + \ldots \tag{9a}$$

$$D_P = D_P^0\theta + \ldots \tag{9b}$$

The first virial coefficients $D_I^0 = A_I(0)$ and $D_P^0 = A_P(0)$ do not depend on the particle distribution. Their values, evaluated in ref 26, using the cluster expansion method, are listed in the first row of Table 1.

Our numerical data presented in Table 1 and the plots of D_I and D_P depicted in Figure 3 (open circles for the square and open triangles for the hexagonal particle lattice) show that for both ordered particle arrangements, the results are nearly identical. The data for the interface contribution are nearly the same (the differences are close to the calculation error), and the results for the particle contributions differ by less than 0.02, with the largest differences occurring at high area fractions. A similar behavior was found in numerical simulations of equilibrium and RSA arrangements of the adsorbed particles, i.e., the streaming current contributions for these random distributions are nearly indistinguishable (see the data in Table 1 and Figure 4 of ref 27).

To facilitate a comparison of our present results for particles placed on a periodic lattice with the earlier calculations for random particle distributions, Figure 3 shows our numerical data for square and hexagonal lattices (symbols) along with the cumulant approximation

$$D_I^{eq} = e^{-D_I^0\theta} \tag{10a}$$

and linear−cumulant approximation

$$D_P^{eq} = a^{eq}\theta + b^{eq}(1 - e^{-D_I^0\theta}) \tag{10b}$$

https://doi.org/10.1021/acsomega.3c05603
ACS Omega 2023, 8, 44717−44723

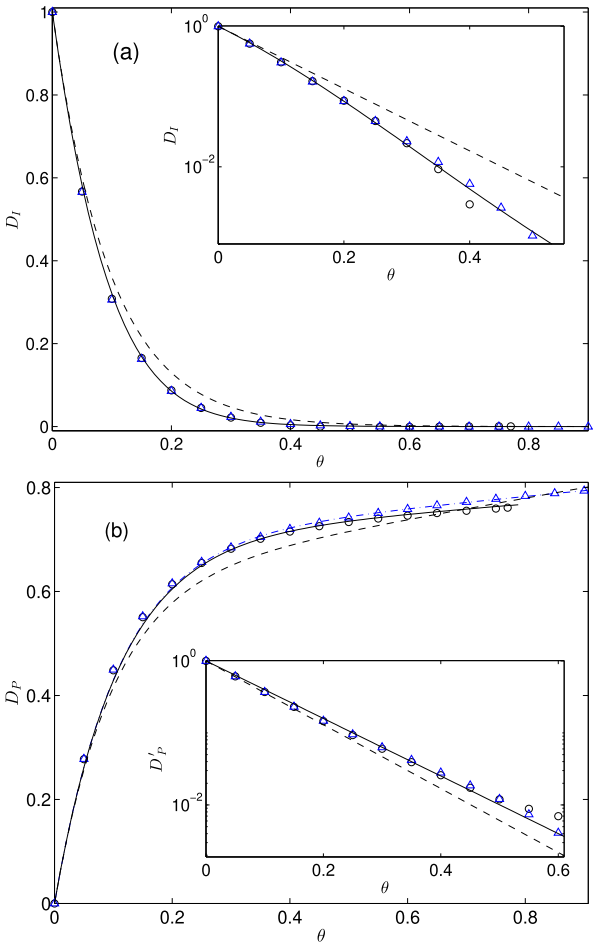

Figure 3. (a) Interface contribution D_I and (b) particle contribution D_P to the streaming current, shown vs the area fraction θ for a square (circles) and hexagonal (triangles) periodic lattice. (a) Solid line represents the cumulant-like approximate eq 12 for ordered particle distributions. The corresponding cumulant approximate eq 10a for random distributions is represented by the dashed line. The inset shows the data in the semilogarithmic scale. (b) Solid line represents the linear−exponential approximation given by eq 13 with the parameters listed in eqs 15 and 17 for the square particle lattice, and the dash−dot line shows approximation from eqs 13 with 16 and 17 for the hexagonal lattice. The dashed line represents the corresponding eq 10b for the random particle distributions. The inset shows the particle contribution to the streaming current with the subtracted linear part, D'_P, (as defined by eq 18), to demonstrate the exponential approach to the linear behavior.

for the interface and particle contributions to the streaming current for the random distributions[27] (dashed lines). The coefficients

$$a^{eq} = 0.202, \qquad b^{eq} = \frac{D_P^0 - a^{eq}}{D_I^0} = 0.6182 \tag{11}$$

in the above expression have been obtained by fitting eq 10b to the numerical data, and D_I^0 and D_P^0 are the first virial coefficients (which are independent of the particle distribution). Both approximations given by eqs 10a and 10b are consistent with the first-order virial expansion from eqs 9a and 9b.

We will now discuss the streaming current for the ordered particle distributions. First we focus on the behavior of the interface contribution to the streaming current D_I. A

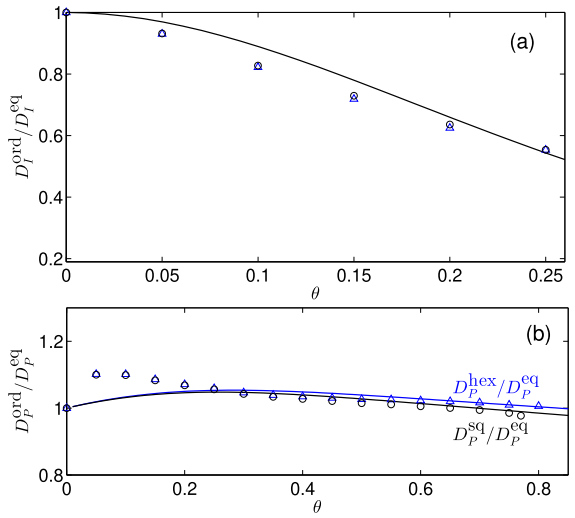

Figure 4. Comparison between the streaming current contributions for the ordered and random particle distributions. (a) Ratio D_I^{ord}/D_I^{eq} between the interface streaming-current contribution for the hexagonal particle lattice, $D_I^{ord} = D_I^{hex}$, (triangles) or square particle lattice, $D_I^{ord} = D_I^{sq}$, (circles) and the equilibrium contribution D_I^{eq}. The solid line shows the ratio between the corresponding phenomenological approximations given by eqs 12, 10a and 10b. (b) Same as panel (a), except that the results are plotted for the particle distribution D_P. The phenomenological expressions in this case are given by eq 10b for the equilibrium distribution and by eq 13 for the hexagonal and square distributions with the corresponding values from eqs 16 and 15 of parameters a and b.

comparison between our present numerical data for the ordered lattices with the cumulant approximation for the equilibrium/RSA particle distributions indicates that for both systems, the function $D_I(\theta)$ decays exponentially with the area fraction. As explained in ref 27, the rapid decay of D_I stems from hydrodynamic screening of the flow near the interface by the adsorbed particles.

The initial decay rate is the same for the ordered and random cases because the first virial coefficient in expansion given by eq 9a does not depend on the particle distribution. However, for larger values of θ, the decay of D_I for ordered particle arrangements is up to 35% faster than that for the random distribution (the inset is shown in Figure 3a). This behavior implies that the hydrodynamic screening is more efficient for ordered than random distributions. The weaker screening by the random distributions (equilibrium and RSA) likely stems from the fact that in the random systems, the empty areas between particles are polydisperse.

In order to account for the variation of the decay rate of D_I with θ for the ordered distributions, we propose a simple approximation

$$D_I^{sq} = D_I^{hex} = e^{-(D_I^0\theta + c_1\theta^2 + c_2\theta^3)} \tag{12}$$

represented by the solid line in Figure 3a. The previously evaluated[26] leading-order virial coefficient $D_I^0 = A_I(0)$ is listed in Table 1, and the parameters $c_1 = -c_2 = 13$ have been obtained from a fit to the numerical data. The expression in eq 12 has a form of the $O(\theta^3)$ cumulant expansion and is based on the approximately linear dependence of log D_I on θ (see the inset of Figure 3a), which results from hydrodynamic screening of the flow field near the interface. The corrections to the linear behavior are accounted for by the square and cubic

https://doi.org/10.1021/acsomega.3c05603
ACS Omega 2023, 8, 44717−44723

terms. For low area fractions $\theta < 0.2$, the absolute accuracy of the approximation given in eq 12 is better than ± 0.02, for higher area fractions $\theta \geq 0.2$ (where D_I has already significantly decayed), the absolute precision is better than ± 0.003.

In contrast to the interface contribution D_I, particle contribution D_P monotonically grows with the increasing area fraction (Figure 3b). The initial growth rate is large, consistent with the value $D_P^0 = 6.510$ of the virial-expansion coefficient. At higher area fractions, however, the growth rate is much lower because only particle areas exposed to external flow contribute to the streaming current.

This behavior is well reflected by a combination of a linear and an exponential function

$$D_P = a\theta + b(1 - e^{-w\theta}) \tag{13}$$

where a and w are fitting parameters and

$$b = (D_P^0 - a)/w \tag{14}$$

for consistency with the virial expansion in eq 9b. By matching the expression in eq 13 to our simulation data, we find

$$a = 0.088, \qquad b = 0.698 \tag{15}$$

for the square lattice and

$$a = 0.109, \qquad b = 0.696 \tag{16}$$

for the hexagonal lattice, with

$$w = 9.2 \tag{17}$$

for both the square and hexagonal particle arrangements. The fitting relation in eq 13 is analogous to the expression from eq 10b for the random particle distribution,[27] but both the linear slope a and the exponential decay rate w are different. The absolute precision of the approximation given by eq 13 with the parameter values listed in eqs 15−17 is better than ± 0.02 for $\theta < 0.25$ and better than ± 0.005 for $\theta \geq 0.25$, for both the hexagonal and square lattices.

The exponential approach to the linear behavior, as described by eq 13, is depicted in the inset of Figure 3*b*, where we plot the function

$$D_P' = 1 - (D_P - a\theta)/b \tag{18}$$

(i.e., D_P with the subtracted linear term) for the square and hexagonal particle distributions along with the exponential fitting function $D_P' = e^{-w\theta}$ (solid line) and the corresponding approximation $D_P' = e^{-D_I^0\theta}$ for the random distribution (dashed line). The results show that the approach of D_P to the linear behavior is slower for the ordered distributions compared to the random distributions, but for square and hexagonal lattices, the exponent is the same.

According to the data shown in Figure 3, the absolute difference between the streaming-current contributions for the periodic and random particle arrangements is small (less than 0.065 and 0.045 for D_I and D_P, respectively, which remains within the usual experimental accuracy). The largest difference occurs in the domain of moderate particle coverage, $0.1 \lesssim \theta \lesssim 0.2$. While the relative difference between the periodic and random results for D_I can be quite large outside the low-area-fraction region (Figure 4), this behavior occurs only when D_I is strongly reduced as a result of hydrodynamic screening. Therefore, in most cases, this difference does not have experimental significance.

The numerical results presented here support our earlier conclusion[27] that surface roughness can significantly reduce the streaming current as long as the Debye length λ is much smaller than the radius of the roughness asperities a_0. Such a rough surface can be modeled as a smooth interface with an attached infinite array of spherical roughness asperities with the same ζ-potential as the underlying interface. Our results for ordered particle monolayers, depicted in Figure 5, show that

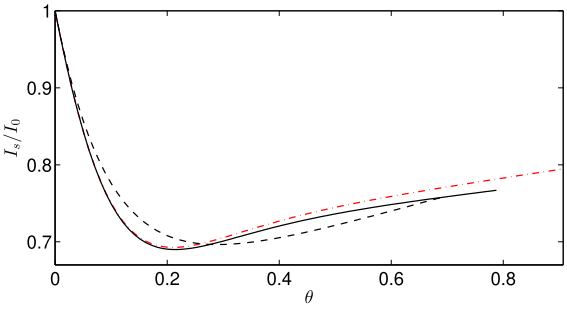

Figure 5. Reduction of the streaming current I_s for a rough surface with spherical asperities relative to the corresponding result I_0 for a smooth surface with the same ζ-potential. The normalized streaming current I_s/I_0 is plotted vs the area fraction θ for the square (solid black line), hexagonal (dashed-dotted red line), and equilibrium/RSA (dashed black line) asperity arrangements.

the streaming current is significantly smaller for a rough surface (up to about 30%) than that for a smooth surface made from the same material. This result generalizes our earlier finding for equilibrium and RSA distributions.[27] We observe that the streaming-current reduction is relatively insensitive to the asperity arrangement, with differences smaller than 5% between I_s/I_0 for the square, hexagonal, and random distributions.

The streaming-current reduction by roughness is a general, universal phenomenon and is important for a correct interpretation of experiments.[27] Since our results do not depend on the particle diameter, this reduction does not vanish when the size of roughness asperities is decreased (as long as the condition $\lambda \ll a_0$ is satisfied). Based on the above observations, we hypothesize that a similar mechanism may decrease the electrokinetic mobility of rough particles.

In conclusion, we have evaluated the interface and particle contributions, D_I and D_P, to the streaming current for interfaces covered by hexagonal and square lattices formed by monolayers of spherical particles. To this end, we have used the accurate methods[38,39,41] based on the multipole expansion of the Stokes equations to evaluate the charge convected by the flow.

We have shown that for both hexagonal and square particle arrangements, the interface contribution D_I can be approximated by a single exponential function with the $O(\theta^3)$ exponent. This function is the same for both lattices, and it decays to zero at large area fractions. The particle contribution D_P can be described by a combination of a linearly increasing term and an exponentially decaying function.

The exponential decay of D_I and the exponentially decaying contribution in D_P stem from the hydrodynamic screening by the particle monolayer. The screening results in a significant reduction of the flow under the particles and the gaps between particles. We find that the screening is more effective for the periodic (square and hexagonal) than random (equilibrium

https://doi.org/10.1021/acsomega.3c05603
ACS Omega 2023, 8, 44717−44723

and RSA) distributions. The weaker screening by the random distributions is likely due to the fact that in the random systems, the empty spaces between particles are polydisperse, and in the larger spaces, the screening is weaker, impeding the overall screening effect.

The linear behavior of D_P at large area fractions is associated with charge convection along the portions of particle surface areas that are exposed to the external flow. The total exposed area is proportional to the number of the adsorbed particles, leading to the linear increase of the streaming current in dense systems (i.e., systems where the flow near the unexposed portions of particle surfaces are already screened out).

Our numerical results and the fitting functions describing D_P, shown in eqs 10b and 13, indicate that the slope a of the linear function to which D_P tends at large area fractions is the largest for the random distributions and the smallest for the square lattice. This dependence may be related to a different effective particle area exposed to the flow, which is influenced by the distribution of the particle neighbors.

In general, we have found that the differences in D_I and D_P between the square and hexagonal lattices are small. The differences between the ordered and random distributions are larger but still not significant. As a result, the normalized streaming current I_s/I_0 is almost insensitive to the specific form of the particle distribution in the adsorbed monolayer.

This is an important finding because it shows that streaming-current measurements can be reliably used to monitor the particle area fraction in a particle monolayer adsorbed on a flat surface. The above conclusion is valid for spherical particles provided that the particle distribution does not involve large density fluctuations (e.g., formation of dense clusters separated by empty or low-density regions). If there are no such fluctuations, detailed information about the particle arrangement is not necessary for the interpretation of the streaming-current measurement results. The usefulness of the streaming-current-based surface-coverage monitoring method is enhanced by the fact that our theoretical findings can be summarized by using simple phenomenological expressions to facilitate the analysis of experimental data.

AUTHOR INFORMATION

Corresponding Authors

Jerzy Blawzdziewicz − *Department of Mechanical Engineering and Department of Physics and Astronomy, Texas Tech University, Lubbock, Texas 79409, United States;* orcid.org/0000-0002-2446-3654; Email: jerzy.blawzdziewicz@ttu.edu

Maria L. Ekiel-Jeżewska − *Institute of Fundamental Technological Research, Polish Academy of Sciences, Warsaw 02-106, Poland;* orcid.org/0000-0003-3134-460X; Email: mekiel@ippt.pan.pl

Author

Zbigniew Adamczyk − *Jerzy Haber Institute of Catalysis and Surface Chemistry, Polish Academy of Sciences, Kraków 30-239, Poland;* orcid.org/0000-0002-8358-3656

Complete contact information is available at: https://pubs.acs.org/10.1021/acsomega.3c05603

Notes

The authors declare no competing financial interest.

ACKNOWLEDGMENTS

M.L.E.-J. was partially supported by the Statutory Activity Fund of the Institute of Technological Research, Polish Academy of Sciences. Z.A. was partially funded by the Statutory Activity Fund of the Jerzy Haber Institute of Catalysis and Surface Chemistry, Polish Academy of Sciences.

REFERENCES

(1) Ramsden, J. J. Experimental methods for investigating protein adsorption kinetics at surfaces. *Q. Rev. Biophys.* **1994**, *27*, 41−105.

(2) Delgado, A. V.; González-Caballero, F.; Hunter, R.; Koopal, L.; Lyklema, J. Measurement and interpretation of electrokinetic phenomena. *J. Colloid Interface Sci.* **2007**, *309*, 194−224.

(3) Adamczyk, Z.; Sadlej, K.; Wajnryb, E.; Nattich, M.; Ekiel-Jeżewska, M.; Blawzdziewicz, J. Streaming potential studies of colloid, polyelectrolyte and protein deposition. *Adv. Colloid Interface Sci.* **2010**, *153*, 1−29.

(4) Lotito, V.; Zambelli, T. Approaches to self-assembly of colloidal monolayers: A guide for nanotechnologists. *Adv. Colloid Interface Sci.* **2017**, *246*, 217−274.

(5) Liang, X.; Dong, R.; Ho, J. C. Self-Assembly of Colloidal Spheres toward Fabrication of Hierarchical and Periodic Nanostructures for Technological Applications. *Adv. Mater. Technol.* **2019**, *4*, 1800541.

(6) Adamczyk, Z.; Dan, N. Editorial overview: Theory and simulation of proteins at interfaces: how physics comes to life. *Curr. Opin. Colloid Interface Sci.* **2019**, *41*, A1−A3.

(7) Adamczyk, Z.; Nattich-Rak, M. *Encyclopedia of Colloid and Interface Science*; Tadros, T., Ed.; Springer Verlang: Berlin Heidelberg, 2013; Chapter 126, pp 868−910.

(8) Adamczyk, Z.; Nattich, M.; Wasilewska, M.; Zaucha, M. Colloid particle and protein deposition — Electrokinetic studies. *Adv. Colloid Interface Sci.* **2011**, *168*, 3−28.

(9) Oćwieja, M.; Adamczyk, Z.; Morga, M.; Kubiak, K. Silver particle monolayers — Formation, stability, applications. *Adv. Colloid Interface Sci.* **2015**, *222*, 530−563.

(10) Lotito, V.; Zambelli, T. Pattern detection in colloidal assembly: A mosaic of analysis techniques. *Adv. Colloid Interface Sci.* **2020**, *284*, 102252.

(11) Malmsten, M. Ellipsometry Studies of Protein Layers Adsorbed at Hydrophobic Surfaces. *J. Colloid Interface Sci.* **1994**, *166*, 333−342.

(12) Buijs, J.; van den Berg, P. A.; Lichtenbelt, J. W.; Norde, W.; Lyklema, J. Adsorption Dynamics of IgG and Its F(ab′)2and Fc Fragments Studied by Reflectometry. *J. Colloid Interface Sci.* **1996**, *178*, 594−605.

(13) Buijs, J.; White, D. D.; Norde, W. The effect of adsorption on the antigen binding by IgG and its F(ab′)2 fragments. *Colloids Surf., B* **1997**, *8*, 239−249.

(14) Michel, R.; Reviakine, I.; Sutherland, D.; Fokas, C.; Csucs, G.; Danuser, G.; Spencer, N. D.; Textor, M. A Novel Approach To Produce Biologically Relevant Chemical Patterns at the Nanometer Scale: Selective Molecular Assembly Patterning Combined with Colloidal Lithography. *Langmuir* **2002**, *18*, 8580−8586.

(15) Sahu, S. S.; Cavallaro, S.; Hååg, P.; Nagy, A.; Karlstrom, A. E.; Lewensohn, R.; Viktorsson, K.; Linnros, J.; Dev, A. Exploiting Electrostatic Interaction for Highly Sensitive Detection of Tumor-Derived Extracellular Vesicles by an Electrokinetic Sensor. *ACS Appl. Mater. Interfaces* **2021**, *13*, 42513−42521.

(16) Sahu, S. S.; Stiller, C.; Gomero, E. P.; Nagy, A.; Karlström, A. E.; Linnros, J.; Dev, A. Electrokinetic sandwich assay and DNA mediated charge amplification for enhanced sensitivity and specificity. *Biosens. Bioelectron.* **2021**, *176*, 112917.

(17) Sahu, S. S.; Gevari, M. T.; Nagy, A.; Gestin, M.; Hååg, P.; Lewensohn, R.; Viktorsson, K.; Karlström, A. E.; Dev, A. Multi-marker profiling of extracellular vesicles using streaming current and sequential electrostatic labeling. *Biosens. Bioelectron.* **2023**, *227*, 115142.

(18) Kumar, A.; Gilson, L.; Henrich, F.; Dahl, V.; Kleinen, J.; Gambaryan-Roisman, T.; Venzmer, J. Intact deposition of cationic

vesicles on anionic cellulose fibers: Role of vesicle size, polydispersity, and substrate roughness studied via streaming potential measurements. *J. Colloid Interface Sci.* **2016**, *473*, 152−161.
(19) Kumar, A.; Dahl, V.; Kleinen, J.; Gambaryan-Roisman, T.; Venzmer, J. Influence of lipid bilayer phase behavior and substrate roughness on the pathways of intact vesicle deposition: A streaming potential study. *Colloids Surf., A* **2017**, *521*, 302−311.
(20) Lee, S.; Kim, H.-J.; Tian, M.; Khang, G.; Kim, H.-W.; Bae, T.-H.; Lee, J. Silk fibroin-coated polyamide thin-film composite membranes with anti-scaling properties. *Desalination* **2023**, *546*, 116195.
(21) Savaji, K. V.; Niitsoo, O.; Couzis, A. Influence of particle/solid surface zeta potential on particle adsorption kinetics. *J. Colloid Interface Sci.* **2014**, *431*, 165−175.
(22) Harmat, A. L.; Morga, M.; Lutkenhaus, J. L.; Batys, P.; Sammalkorpi, M. Molecular mechanisms of pH-tunable stability and surface coverage of polypeptide films. *Appl. Surf. Sci.* **2023**, *615*, 156331.
(23) Dąbkowska, M.; Adamczyk, Z. Human Serum Albumin Monolayers on Mica: Electrokinetic Characteristics. *Langmuir* **2012**, *28*, 15663−15673.
(24) Dąbkowska, M.; Adamczyk, Z. *J. Colloid Interface Sci.* **2012**, *366*, 105−113.
(25) Adamczyk, Z.; Nattich-Rak, M.; Dąbkowska, M.; Kujda-Kruk, M. Albumin adsorption at solid substrates: A quest for a unified approach. *J. Colloid Interface Sci.* **2018**, *514*, 769−790.
(26) Sadlej, K.; Wajnryb, E.; Blawzdziewicz, J.; Ekiel-Jeżewska, M. L.; Adamczyk, Z. Streaming current and streaming potential for particle covered surfaces: Virial expansion and simulations. *J. Chem. Phys.* **2009**, *130*, 144706.
(27) Ekiel-Jeżewska, M. L.; Adamczyk, Z.; Blawzdziewicz, J. Streaming Current and Effective ζ-Potential for Particle-Covered Surfaces with Random Particle Distributions. *J. Phys. Chem. C* **2019**, *123*, 3517−3531.
(28) Schaaf, P.; Talbot, J. Kinetics of Random Sequential Adsorption. *Phys. Rev. Lett.* **1989**, *62*, 175−178.
(29) Khanh, N. N.; Yoon, K. B. Facile Organization of Colloidal Particles into Large, Perfect One- and Two-Dimensional Arrays by Dry Manual Assembly on Patterned Substrates. *J. Am. Chem. Soc.* **2009**, *131*, 14228−14230.
(30) Lotito, V.; Zambelli, T. Self-assembly and nanosphere lithography for large-area plasmonic patterns on graphene. *J. Colloid Interface Sci.* **2015**, *447*, 202−210.
(31) Solomentsev, Y.; Böhmer, M.; Anderson, J. L. Particle Clustering and Pattern Formation during Electrophoretic Deposition: A Hydrodynamic Model. *Langmuir* **1997**, *13*, 6058−6068.
(32) Gong, T.; Wu, D. T.; Marr, D. W. Two-Dimensional Electrohydrodynamically Induced Colloidal Phases. *Langmuir* **2002**, *18*, 10064−10067.
(33) Cong, H.; Cao, W. Colloidal Crystallization Induced by Capillary Force. *Langmuir* **2003**, *19*, 8177−8181.
(34) Prevo, B. G.; Velev, O. D. Controlled, Rapid Deposition of Structured Coatings from Micro- and Nanoparticle Suspensions. *Langmuir* **2004**, *20*, 2099−2107.
(35) Huang, S.; Minami, K.; Sakaue, H.; Shingubara, S.; Takahagi, T. Effects of the Surface Pressure on the Formation of Langmuir−Blodgett Monolayer of Nanoparticles. *Langmuir* **2004**, *20*, 2274−2276.
(36) Gouy, M. Sur la constitution de la charge électrique à la surface d'un électrolyte. *J. Phys. Theor. Appl.* **1910**, *9*, 457−468.
(37) Chapman, D. L. LI. A contribution to the theory of electrocapillarity. *London, Edinburgh Dublin Phil. Mag. J. Sci.* **1913**, *25*, 475−481.
(38) Cichocki, B.; Felderhof, B. U.; Hinsen, K.; Wajnryb, E.; Blawzdziewicz, J. Friction and mobility of many spheres in Stokes flow. *J. Chem. Phys.* **1994**, *100*, 3780−3790.
(39) Cichocki, B.; Ekiel-Jeżewska, M. L.; Wajnryb, E. Lubrication corrections for three-particle contribution to short-time self-diffusion coefficients in colloidal dispersions. *J. Chem. Phys.* **1999**, *111*, 3265−3273.
(40) Bhattacharya, S.; Blawzdziewicz, J.; Wajnryb, E. Hydrodynamic interactions of spherical particles in suspensions confined between two planar walls. *J. Fluid Mech.* **2005**, *541*, 263−292.
(41) Bhattacharya, S.; Blawzdziewicz, J.; Wajnryb, E. Many-particle hydrodynamic interactions in parallel-wall geometry: Cartesian-representation method. *Phys. Stat. Mech. Appl.* **2005**, *356*, 294−340.
(42) Bhattacharya, S.; Blawzdziewicz, J.; Wajnryb, E. Hydrodynamic interactions of spherical particles in Poiseuille flow between two parallel walls. *Phys. Fluids* **2006**, *18*, 053301.

https://doi.org/10.1021/acsomega.3c05603
ACS Omega 2023, 8, 44717−44723